Korean J. Chem. Eng., 36(3), 368-376 (2019)
DOI: 10.1007/s11814-018-0211-9

pISSN: 0256-1115
eISSN: 1975-7220

Anodic aluminum oxide supported Cu-Zn catalyst for oxidative steam reforming of methanol

Jung Hyeon Kim, Young Shin Jang, Jae Chang Kim, and Dong Hyun Kim†

Department of Chemical Engineering, Kyungpook National University, Daegu 41566, Korea
(*Received 6 October 2018 • accepted 13 December 2018*)

Abstract−Oxidative steam reforming of methanol (OSRM) is autothermal and therefore well suited for hydrogen production. The exothermic part of OSRM generates heat at the reactor inlet to be used as the reaction heat for the endothermic methanol steam reforming in the rest of the reactor. With conventional particle catalysts, a hot spot is formed at the reactor inlet because of the poor thermal conductivity in the catalyst bed. The catalyst at the hot spot is deactivated by thermal sintering. Side reactions such as the reverse water gas shift reaction and methanol decomposition reaction become active at the hot spot. We developed a high-thermal-conductivity Al plate catalyst to suppress the formation of the hot spot in the catalyst bed during OSRM. In particular, a strongly bonded layer of anodic aluminum oxide as a catalyst support was grown on the Al plate surface via anodic oxidation in oxalic acid solution, and the internal surface area of the support was increased by pore widening and hot water treatments. To obtain a catalyst with high activity, multiple impregnations (>three times) and an anodization time of 24 h was needed. The catalyst was deactivated when operated at an elevated temperature of 623 K, but the activity was completely restored by a simple oxidation. Notably, OSRM was proven to be a combination of methanol combustion and methanol steam reforming reactions, and the kinetics of these two reactions were studied in detail.

Keywords: Oxidative Steam Reforming of Methanol, Anodic Aluminum Oxide, Aluminum Plate Catalyst, Methanol Combustion, Methanol Steam Reforming Rate, Methanol Combustion Rate

INTRODUCTION

Commercial fuel-cell cars use hydrogen compressed to a very high pressure of 700 bar. Nevertheless, their driving ranges are still shorter than those of conventional liquid-fuel vehicles because of the low storage density of the compressed hydrogen. In addition, the widespread utilization of such cars is hindered by the need to newly construct the infrastructure of hydrogen refueling stations.

Onboard fuel processing to produce hydrogen for fuel-cell cars has been investigated as a possible way of mitigating the above issues [1,2]. In theory, hydrogen can be produced from any gas-phase or liquid hydrocarbons by steam reforming. However, steam reforming of hydrocarbons other than methanol occurs at temperatures above 873 K and hence generates significant amounts of CO [3-5]. The CO should be converted to CO_2 via the water-gas-shift reaction [2] to produce hydrogen that usually consists of high-temperature and low-temperature shifts. On the other hand, steam reforming of methanol is typically performed at 473-573 K and affords gas mixtures with CO content low enough to avoid the shift reaction stage [6-8], which makes methanol an attractive substrate for simple fuel processors. In the 1990s, early prototype fuel-cell cars were equipped with onboard methanol steam reformers, which, however, exhibited long start up time, short catalyst lifetime, and bulky structure, and hence limited the performance of these vehicles. Thus, the development of onboard fuel processors lagged behind the advancement of fuel cells and other systems, and therefore, fuel cell cars produced in 2010s all utilize compressed hydrogen. Nevertheless, fuel processors without the abovementioned shortcomings would be able to replace the current hydrogen storage in cars and make fuel-cell cars a competitive alternative to conventional ones. In view of the above, we herein aimed to develop a high-performance catalyst for methanol fuel processing suitable for mobile applications.

The steam reforming of methanol (SRM, Eq. (1)) is an endothermic reaction that can be made autothermal by adding O_2 into the feed, which results in the oxidative steam reforming of methanol (OSRM, Eq. (2)):

$$CH_3OH+H_2O\rightarrow CO_2+3H_2 \qquad \Delta H=49\ kJ\ mol^{-1}\ (at\ 298\ K) \quad (1)$$

$$CH_3OH+0.8H_2O+0.1O_2\rightarrow CO_2+2.8H_2 \qquad \Delta H\approx 0\ kJ\ mol^{-1}\ (at\ 298\ K) \quad (2)$$

OSRM obviates the need for external heat supply or removal, and therefore allows the construction of simple and compact reactors exhibiting small heat capacities and therefore capable of quick start-up.

However, in OSRM reactors, the reaction between O_2 and methanol occurs first, and the reaction of methanol with water to produce hydrogen and CO_2 starts only after substantial O_2 conversion [9-11]. Therefore, the heat initially generated at the reactor inlet should be transferred to the rest of the reactor for SRM to occur. In conventional packed-bed reactors, this results in the formation of a hot spot at the inlet, since heat transfer along the catalyst bed is poor, and most of the heat is therefore carried by the gas flow [12,13]. The temperatures of such hot spots were 878 K [12] and

†To whom correspondence should be addressed.
E-mail: dhkim@knu.ac.kr

600-700 K [13], which significantly exceed the safe operating temperature range (473-573 K) of Cu-based catalysts [14]. At hot spots, Cu-based catalysts are deactivated and undesired CO-producing side reactions such as reverse water gas shift reaction and methanol decomposition reaction become active. Hence to avoid the problems, a hot spot must not be formed during OSRM, and the reactors should be capable of very rapid heat transfer to remove the hot spot. One way for removal of the hot spot is the use of monolith reactors made of Al, which exhibits the advantages of low density and high thermal conductivity (237 W m^{-1} K^{-1}) that significantly exceeds that of the catalyst bed (0.2-0.8 W m^{-1} K^{-1}) [15,16] and is therefore well suited for rapid heat transfer along the reactor. Indeed, it was shown that the hot spot was absent in a highly conductive aluminum honeycomb reactor during OSRM [17].

The OSRM catalyst layer comprises metal oxides, mainly CuO and ZnO. Deposition and adherence of the metal oxides on the metal surface of the monolith is not an easy task as there is little interaction between the oxides and the surface metal. A large thermal expansion coefficient of the metal compared to the coefficient of the oxides can lead to cracks and loosening of the catalyst layer. To avoid these problems the adhesion of the catalyst layer to the substrate should be strong.

A layer of self-organized hexagonal pore arrays can be formed by anodic oxidation of aluminum [18-20]. The anodic aluminum oxide (AAO) layer can be grown to over a hundred micrometers in thickness [20,21] and adheres to the substrate aluminum metal strongly [22,23]. The alumina layer has a significant surface area, particularly after a hydrothermal treatment [23,24], and has been a good catalyst support for electro-deposition of Pt [25] and Cu [26, 27]. In this study, AAO supports were prepared and impregnated with Cu and Zn solutions multiple times to obtain a highly active and thermally conductive catalyst for OSRM. The effects of anodization time and the subsequent treatments after the anodization on the properties of the supports as well as on the catalyst activity after the impregnations were investigated. For the AAO catalyst, the reaction rate of OSRM in terms of the rate of SRM and the rate of methanol combustion was also obtained.

EXPERIMENTAL

1. Catalyst Support

An Al plate (10 cm×12 cm, thickness=0.5 mm, purity=99.9%) was washed with 0.1 N nitric acid and distilled water, annealed at 673 K for 3 h to remove internal stresses, and anodized for 12, 24, or 48 h in 0.3 M oxalic acid at 40-V DC and 283 K using a graphite plate as a cathode [23,27]. Subsequently, the AAO plate was subjected to pore-widening treatment (PWT) by 4-h immersion into the abovementioned oxalic acid solution at 303 K, which resulted in the dissolution of alumina on pore walls [27-29]. After PWT, the AAO plate was put into hot deionized water at 368 K for 1 h (hot water treatment, HWT) to increase the surface area of the AAO layer [23,26,27,30], and the thus treated AAO plates were calcined at 673 K for 3 h.

2. Impregnation

For impregnation, the AAO plate was immersed into a solution of $Cu(NO_3)_2 \cdot 3H_2O$ and $Zn(NO_3)_2 \cdot 6H_2O$ (both 1 M) for 5 min or 1 h, and excess nitrate solution was subsequently removed from the plate surface by compressed air blow-off. The impregnated plate was dried at 353 K for 24 h, calcined at 673 K for 3 h in air, and subjected to a new round of impregnation-drying-calcination up to a total of five rounds. Thus obtained catalysts (prepared by 24-h anodization followed by PWT and HWT) were denoted as Cu-Zn(*N*)/AAO(24 h, PWT-HWT), where *N* is the number of impregnation cycles.

3. Reactor and Activity Measurement

The catalyst plate was cut into strips of 2×20 mm, and 50 strips were packed into a quartz tube (12.7 mm OD, 10.6 mm ID) to afford a total catalytic plate area of 4×10^{-3} m^2 in the reactor. A thermocouple was inserted into the center of the bed to measure reactor temperature (T_R), and the catalyst was reduced in a 10% H_2/He stream at 523 K for 2 h before the reaction. Methanol and water saturators were used to vaporize the reactants, and the resulting vapors were transported to the reactor using helium as a carrier gas. The temperature of each saturator was controlled by a circulating water bath. SRM and OSRM were performed using 15% CH_3OH - 25% H_2O - balance He and 3% O_2 - 15% CH_3OH - 25% H_2O - balance He feeds, respectively. The total flow rate was set to 100 mL (STP) min^{-1}. Effluent gases were analyzed online by a gas chromatograph (HP 5890A) equipped with thermal conductivity detectors. A Porapak Q column was used for separation of CO_2, CH_3OH, and H_2O, and a Caboxen column for separation of O_2, CO, and CO_2. The products in the reactor effluent were H_2 and CO_2 with CO not exceeding 1% for reaction temperatures below 573 K, and no other products were observed.

To examine the thermal stability of catalyst activity, the reactor temperature was cycled between 523 and 623 K, with each cycle comprising 1 h at 523 K and 3 h at 623 K.

4. Cu Area

The Cu metal area of the catalyst was measured by N_2O chemisorption (Eq. (3)) [31].

$$2\,Cu_{(s)} + N_2O \rightarrow Cu_2O_{(s)} + N_2 \quad (3)$$

The catalyst plate was reduced at 523 K for 3 h in a flow of 10% H_2/N_2 (50 mL min^{-1}), and the reactor was cooled to 353 K in a flow of N_2 (20 mL min^{-1}). Subsequently, 20 μL N_2O pulses were injected in 3-min intervals into the N_2 stream flowing through the reactor through a six-port valve. For each injected pulse, the peak with *m/z* 44 for N_2O in the reactor effluent was monitored by a mass spectrometer (Pfeiffer Vacuum QME200). The initial 3-4 N_2O pulses were completely consumed in the reactor, i.e., no N_2O peaks were detected at the exit, whereas pulses with progressively increasing intensity were detected subsequently. The amount of N_2O consumed by the catalyst was calculated as the total injected amount minus the total amount eluted from the reactor. A value of 1.46×10^{19} Cu atoms m^{-2} was used to estimate the Cu metal area of the catalyst [31]. The Cu area per 1 m^2 of the AAO plate area (S_{Cu}) was determined.

RESULTS AND DISCUSSION

1. Characterization

Fig. 1 shows scanning electron microscopy (Hitachi SU8220)

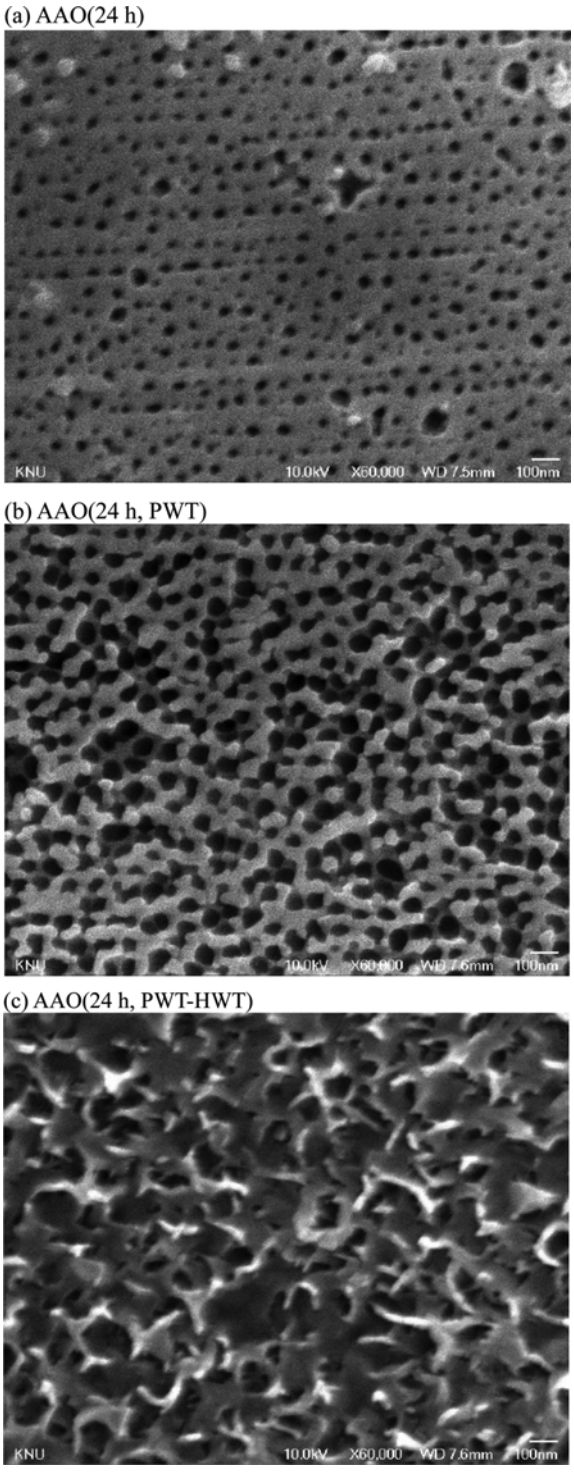

Fig. 1. SEM images of AAO plates obtained after (a) 24-h anodization followed by 3-h calcination at 673 K, (b) 24-h anodization followed by PWT and 3-h calcination at 673 K, and (c) 24-h anodization followed by PWT-HWT and 3-h calcination at 673 K.

images of AAO plates subjected to processing under different conditions, and Table 1 lists the corresponding physical properties measured with Micromeritics ASAP 2010. The surface area per unit weight (S_g) increased from 0.88 to 3.88 $m^2 g^{-1}$ as the anodization time increased from 12 to 48 h. Whereas PWT resulted in a pore size increase, HWT was most significant in increasing the internal surface area more than a factor of 10 [23,26,27,30]. The thickness of the AAO(24 h, PWT-HWT) layer was 70 μm on both sides of the plate in which the thickness of the Al metal was 350 μm (not shown). Table 1 also lists specific surface areas per m^2 of Al plate area, S_p, for comparison of internal surface area with AAO plate area. For example, the internal surface area of AAO(24 h, PWT-HWT) was 27,100 m^2 per m^2 of the plate area. Fig. 2 shows the pore size distributions of AAO supports, demonstrating that pores initially formed during anodization had a diameter of ~30 nm that increased to an average of 47 nm after PWT, which also resulted in pore size distribution broadening. Notably, HWT induced pore collapse, forming very small (average diameter=4 nm) pores, and at the same time increasing the internal surface area greatly.

Table 1. Physical properties of anodic aluminum oxide (AAO) plates

	S_g ($m^2 g^{-1}$)	S_p*	Pore volume ($cm^3 g^{-1}$)	Pore size (nm)
AAO(12 h)	0.88	600	0.008	24
AAO(12 h, PWT-HWT)	28.7	18400	0.022	3.2
AAO(24 h)	1.28	830	0.016	30
AAO(24 h, PWT)	2.79	1810	0.021	47
AAO(24 h, PWT-HWT)	42.9	27100	0.047	4.0
AAO(48 h)	3.88	2620	0.028	35
AAO(48 h, PWT-HWT)	68.6	40000	0.058	3.5

*Specific surface area per m^2 plate area (dimensionless)

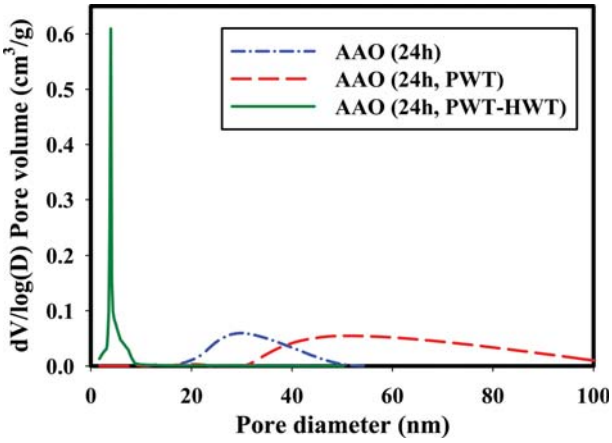

Fig. 2. Pore size distributions of AAO supports.

Fig. 3 shows SEM images of the catalyst plate surface, showing that the extent of metal oxide coverage increased with the number of impregnations, *N*. For the catalyst with *N*=3, the surface compositions of metal oxide-covered (A in Fig. 4) and metal oxide-free (B in Fig. 4) parts were determined by energy-dispersive X-ray spectroscopy (Hitachi SU8220) and listed in Table 2. The EDX showed that the Cu contents of these regions (A: 43.5 at%, B: 4.2 at%) were significantly different, i.e., region A mainly corresponded to CuO.

Although the concentrations of Zn and Cu nitrates in the solution used for impregnation were identical, the Cu content of regions

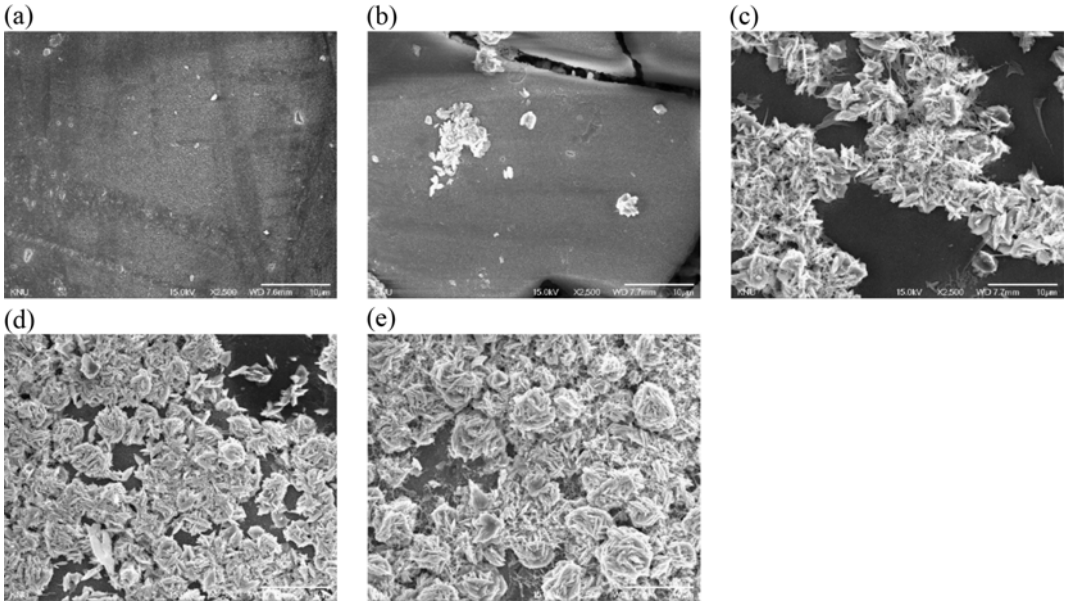

Fig. 3. SEM images of (a) Cu-Zn(1)/AAO(24 h, PWT-HWT), (b) Cu-Zn(2)/AAO(24 h, PWT-HWT), (c) Cu-Zn(3)/AAO(24 h, PWT-HWT), (d) Cu-Zn(4)/AAO(24 h, PWT-HWT), and (e) Cu-Zn(5)/AAO(24 h, PWT-HWT).

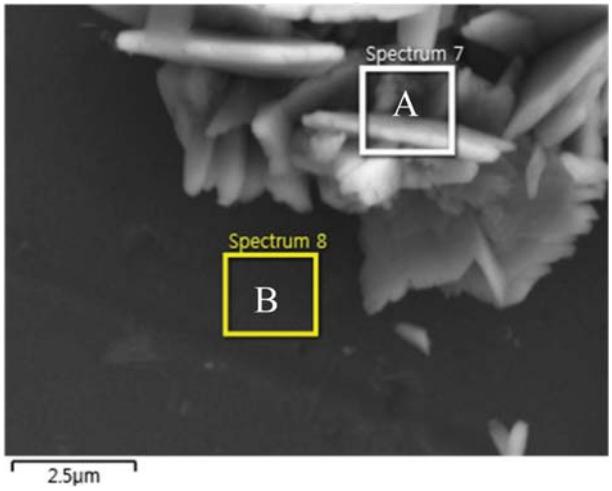

Fig. 4. Areas used for the EDX analysis of Cu-Zn(3)/AAO(24 h, PWT-HWT).

A and B significantly exceeded the corresponding Zn contents. This unexpected result was difficult to explain, as impregnation in general is considered to be non-selective, but indicated that Cu species had a higher affinity to the AAO plate than Zn species.

Table 2 lists the elemental compositions of catalysts measured by EDX analysis of AAO layer cross-sections for different values of *N*, showing that the loadings of Cu and Zn increased with increasing *N*, with that of Cu exceeding that of Zn at identical *N*. The interior Cu content for *N*=3 (4.4 at%) resembled that of the outer surface of the AAO layer not covered with metal oxide clusters (region B in Fig. 4, 4.2 at%). Cu areas measured as described in section 2.4 (Table 2) increased with increasing Cu loading, i.e., with increasing *N*.

2. Catalyst Activity

AAO catalysts were tested for SRM to compare catalytic activity. The reactor effluent was a mixture of H_2, CO_2, unreacted CH_3OH and H_2O, and CO less than 1% when the reactor temperature was lower than 573 K. The CO in the mixture was shown to be formed

Table 2. Results of SEM-EDX composition analysis and Cu area of AAO catalysts

	Content (at%)				Cu area, S_{Cu} ($m^2\ m^{-2}$)
	O	Al	Cu	Zn	
Surface composition					
Region A in Fig. 4	51.8	2.1	43.5	2.6	-
Region B in Fig. 4	60.1	34.4	4.2	1.3	-
Interior composition					
Cu-Zn(1)/AAO(24 h, PWT-HWT)	70.2	27.8	1.4	0.6	216
Cu-Zn(2)/AAO(24 h, PWT-HWT)	70.1	26.5	2.5	0.9	675
Cu-Zn(3)/AAO(24 h, PWT-HWT)	66.2	28.2	4.4	1.2	745
Cu-Zn(4)/AAO(24 h, PWT-HWT)	68.4	24.8	5.3	1.5	892
Cu-Zn(5)/AAO(24 h, PWT-HWT)	65.7	26.3	6.2	1.8	1030

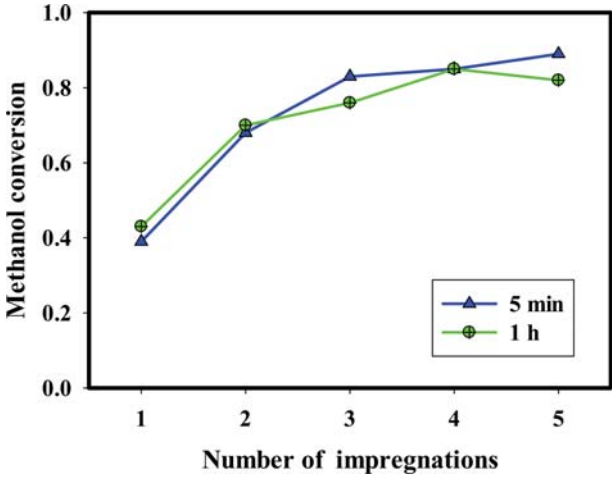

Fig. 5. Effect of impregnation time (5 min or 1 h) and number of impregnations (N=1-5) on the conversion of methanol in SRM. T_R=523 K, feed: 15% CH_3OH, 25% H_2O, and balance He (100 mL (STP) min^{-1}).

by the reverse water-gas-shift reaction [7].

Fig. 5 shows the effects of *N* and impregnation time (5 min or 1 h) on the activity of the catalyst supported by AAO(24 h, PWT-HWT), showing that although methanol conversion increased with *N*, this increase became progressively less pronounced for *N*>3. On the other hand, the impregnation time of 5 min or 1 h had little difference in the catalyst activities. The impregnation time of 5 min was employed in the subsequent catalyst preparations.

Most Cu catalysts need to be operated below 573 K to avoid the rapid sintering of Cu species [14]. Nevertheless, the reaction temperature was raised to 623 K to expedite catalyst deactivation and examine the thermal stability of catalyst activity. Since most catalysts achieved complete methanol conversion at 623 K, the reaction temperature was lowered to 523 K to obtain conversions of less than 1.0 and thus compare catalyst activity. Thermal cycling as described in section 2.3. (1 h at 523 K and 3 h at 623 K) was performed for 33 h, and the corresponding methanol conversion changes are shown in Fig. 6. Depending on the number of impregnation cycles (*N*), the catalysts showed different deactivation behavior. For *N*=1, the methanol conversion at 523 K was 0.39. After 1 h at 523 K, the reactor temperature was raised to 623 K in 7 min, and the conversion concomitantly increased to 0.98, decreasing to 0.91 after 3 h at 623 K. Subsequently, the reactor temperature was decreased to 523 K in 10 min, and the conversion further decreased to 0.22. After four such temperature cycles, the conversion at 523 K dropped to 0.02, which was indicative of severe deactivation. For *N*=5, however, the methanol conversion decreased from 0.90 to 0.65 in the first four cycles, which indicated a much higher thermal stability than in the case of *N*=1. Notably, the increase of methanol conversion became less marked for *N*≥3.

At the end of temperature cycling, the Cu metal area of Cu-Zn(5)/AAO(24 h, PWT-HWT) was measured as described in section 2.4., and the value was 424 after eight cycles, which was much less than that of the fresh catalyst (S_{Cu}=1030), indicating the occurrence of significant Cu sintering.

Fig. 7 shows the effect of anodization time (12, 24, and 48 h) on the activity of *N*=5 PWT-HWT catalysts subjected to the same number of temperature cycles, demonstrating that a significant increase of catalytic activity was observed when the anodization time was increased from 12 to 24 h, but a further extension to 48 h had no large effect.

Finally, we evaluated the long-term stability of catalytic activity for SRM and OSRM (Fig. 8). The furnace temperature was set to 523 K, and T_R for SRM was measured as 515 K because of the endothermicity of this reaction. Conversely, a higher T_R was measured for the exothermic OSRM process (533 K), which accounted for the fact that the conversion of methanol in OSRM exceeded that in SRM. For both reactions, the activity of the catalyst was stabilized after an initial equilibration period of 40-60 h.

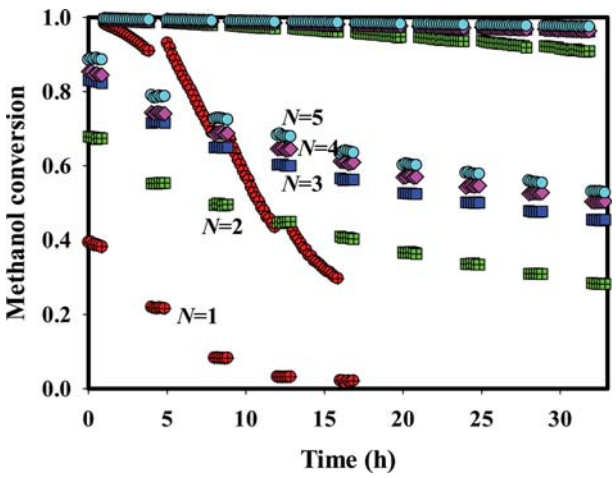

Fig. 6. Methanol conversion over AAO catalysts in SRM as a function of reaction time during temperature cycling. In each temperature cycle, the temperature was 523 K for 1 h followed by 623 K for 3 h. N is the number of impregnations.

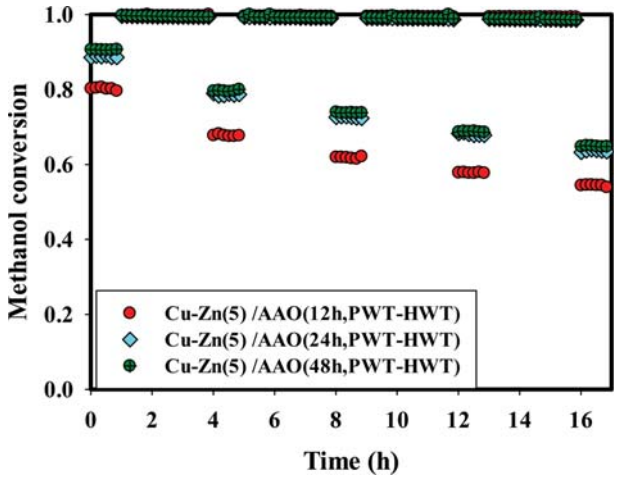

Fig. 7. Methanol conversion over AAO catalysts prepared using different anodization times as a function of time during temperature cycling. In each temperature cycle, the temperature was 523 K for 1 h followed by 623 K for 3 h.

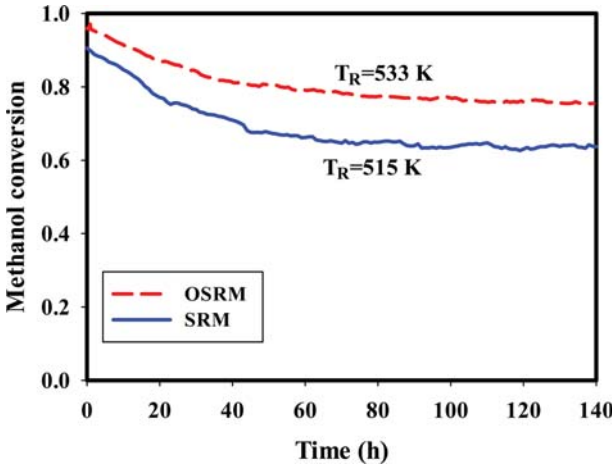

Fig. 8. Methanol conversion as a function of time for SRM (T_R=515 K) and OSRM (T_R=533 K). Catalyst: Cu-Zn(5)/AAO(24 h, PWT-HWT).

3. Catalyst Reactivation

After the temperature cycling (Fig. 6), the Cu metal area of Cu-Zn(5)/AAO(24 h, PWT-HWT) decreased to 424 from 1030 of the fresh catalyst. The sintered catalyst was oxidized in a flow of 10% O_2/He at 523 K for 30 min, and the Cu metal area of the oxidized catalyst was measured as 1241, which exceeded the value of the fresh catalyst (S_{Cu}=1030). At the same time, oxidation resulted in an increase in methanol conversion (at 523 K) from 0.54 to 0.91. The reactivated catalyst was subjected to temperature cycling as described above, and the obtained methanol conversions were equal to or greater than those observed for the fresh catalyst (Fig. 9). After eight temperature cycles, the spent reactivated catalyst was re-oxidized, and the methanol conversion at 523 K again returned to 0.91 (a in Fig. 9) from 0.61 (b in Fig. 9). The catalyst used in Fig. 8 was also oxidized after 140 h of time-on-stream, and its activity was also fully recovered (data not shown).

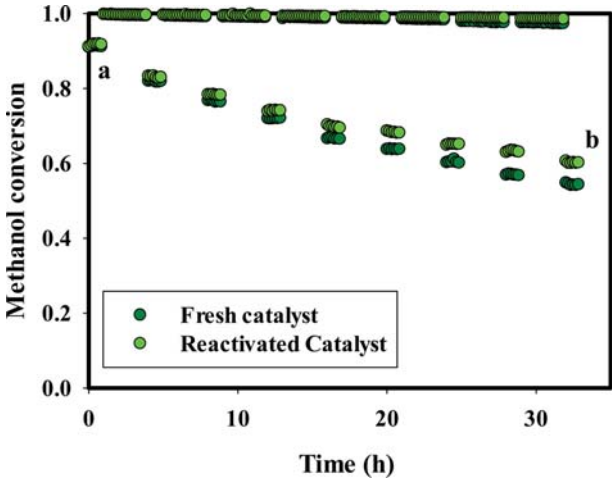

Fig. 9. Methanol conversion over fresh and reactivated AAO catalysts as a function of time during temperature cycling. In each temperature cycle, the temperature was 523 K for 1 h followed by 623 K for 3 h. Catalyst: Cu-Zn(5)/AAO(24 h, PWT-HWT).

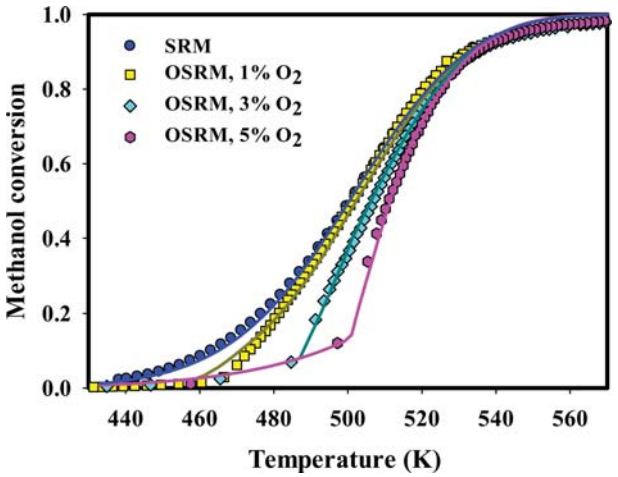

Fig. 10. Methanol conversion over Cu-Zn(5)/AAO(24 h, PWT-HWT) for SRM (0% O_2) and OSRM (1%, 3%, and 5% O_2 in the feed, 100 mL min^{-1}). Lines are methanol conversion calculated using the reactor model (Eqs. (11) and (12)) with SRM (Eqs. (6) and (10)) and COM (Eq. (15)) reaction rates.

Oxidation treatment has been reported to restore the catalytic activity of a Cu catalyst to its initial value for both SRM [32] and OSRM [33], and oxidation of the sintered Cu phase has been reported to regenerate a finely dispersed CuO phase [34]. The Cu area recovery of the plate catalyst after oxidation also showed that oxidation re-dispersed the sintered Cu phase formed at 623 K.

4. OSRM Performance

The feed rates of CH_3OH and H_2O were fixed at 15 and 25 mL min^{-1}, respectively, whereas that of O_2 was varied (0 (SRM), 1, 3, and 5 mL min^{-1}), with the corresponding methanol conversions at 423-573 K shown in Fig. 10. Notably, SRM methanol conversion exceeded the corresponding OSRM value and decreased with increasing oxygen content in the temperature range of 460-520 K.

The reaction between O_2 and CH_3OH has commonly been viewed as the partial oxidation of methanol (POM, Eq. (4)) [35-39]:

$$CH_3OH+0.5O_2 \rightarrow CO_2+2H_2 \quad \Delta H=-192.5\ kJ\ mol^{-1}\ (at\ 298\ K) \quad (4)$$

If POM were the only reaction between methanol and oxygen, CO_2 and H_2 would be produced at all O_2 conversions. However, instead of H_2, formation of H_2O was observed until near-complete O_2 conversion, which indicated that the observed reaction corresponded to the combustion of methanol (COM, Eq. (5)) [33,40,41]:

$$CH_3OH+1.5O_2 \rightarrow CO_2+2H_2O \quad \Delta H=-676.5\ kJ\ mol^{-1}\ (at\ 298\ K) \quad (5)$$

For O_2 and CH_3OH, changes in the entering flow rates and the exiting flow rates through the reactor were negative, as both components were consumed in the reactor. In Fig. 11, the change in O_2 flow rate ($-\Delta O_2$) was plotted against the change in CH_3OH flow rate ($-\Delta CH_3OH$) for three different O_2 feed flow rates (1, 2 and 3 ml/min), and the expected relations between the changes in the flow rates of O_2 and CH_3OH for COM and POM were indicated by lines. For example, $-\Delta O_2$=3 ml/min corresponded to $-\Delta CH_3OH$= 2 ml/min by Eq. (5) or $-\Delta CH_3OH$=6 ml/min by Eq. (4). In the experiments for the data in Fig. 11, the feed flow rates of CH_3OH

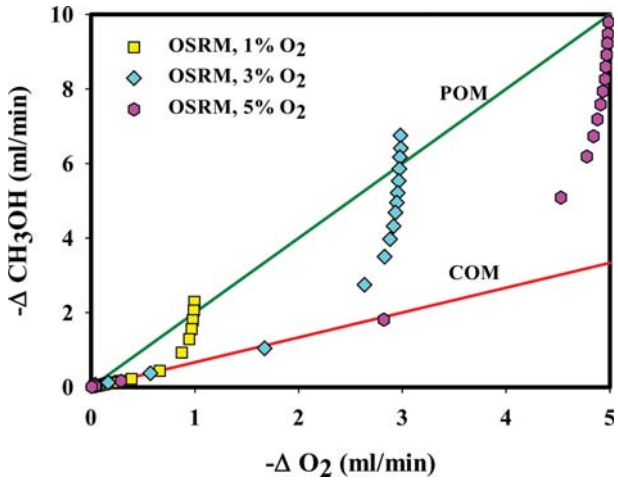

Fig. 11. Plot of the change in the flow rate of O_2 ($-\Delta O_2$) against the change in the methanol flow rate ($-\Delta CH_3OH$) through the reactor. Catalyst: Cu-Zn(5)/AAO(24 h, PWT-HWT). Feed composition: 15 % CH_3OH, 25% H_2O, O_2 (shown) and balance He. Feed flow rate: 100 ml/min.

and H_2O were fixed at 15 and 25 mL min^{-1}, respectively, and He feed flow rate was adjusted to keep the total feed flow rate at 100 ml/min. For each O_2 feed rate, the change in CH_3OH flow rate ($-\Delta CH_3OH$) with respect to the change in O_2 flow rate ($-\Delta O_2$) initially followed COM line, moved upward at O_2 conversions above 0.6, and rose vertically upon complete O_2 conversion, indicating the onset of SRM. In any part of the O_2 conversion range, the data did not followed the POM line, excluding POM from the constituting reactions of OSRM. Therefore, it is proved that OSRM is a combination of COM and SRM. Consequently, the OSRM reaction rate is a combination of the rates of COM and SRM.

5. Rate of SRM over Cu-Zn(5)/AAO(24 h, PWT-HWT)

Initially, we investigated the influence of feed composition on methanol conversion to identify the feed component affecting the reaction rate. The reactor temperature used for these experiments ranged from 433 to 533 K. Fig. 12 shows methanol conversion as a function of reaction temperature for various feed compositions. The total feed flow rate was fixed at 100 mL min^{-1}, and feed compositions were denoted as (M*x* W*y* H*z*), e.g., (M15 W25 H30) corresponded to 15% CH_3OH, 25% H_2O and 30% H_2. The results obtained for (M5 W25), (M10 W25), and (M15 W25) showed that the reactor outlet conversion decreased with increasing methanol concentration in the feed. Addition of H_2 to the feed, as in (M15 W25 H15) and (M15 W25 H30), lowered methanol conversion, whereas the content of H_2O did not affect methanol conversion as long as H_2O was not the limiting reactant (data not shown).

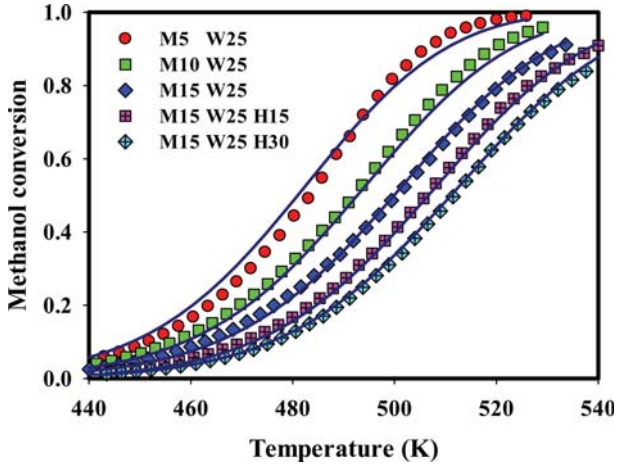

Fig. 12. Methanol conversion as a function of reaction temperature for various feed compositions. Lines are methanol conversion computed using the rate equation Eq. (6) with the fitted parameters of Eq. (10).

Thus, the rate of SRM was only affected by the contents of methanol and hydrogen in the feed, in agreement with the results obtained for SRM over a commercial Cu-Zn catalyst (Synetix 33-5) by Lee et al. [7]. They developed a mechanism of SRM and the resulting reaction rate for the commercial catalyst [7]. It was assumed that the same reaction mechanism could be applied to SRM over the AAO plate catalyst, and hence the same reaction rate form was used to describe the SRM rate over the plate catalyst. The rate form in [7] is

$$-r_M = \frac{k\frac{K_1 P_M}{\sqrt{P_{H_2}}}}{\left(1+\frac{K_1 P_M}{\sqrt{P_{H_2}}}\right)\left(1+\sqrt{K_2 P_{H_2}}\right)} \quad (\text{mol m}^{-2}\,\text{s}^{-1}) \tag{6}$$

where P_M is the partial pressure of methanol (kPa), P_{H_2} is the partial pressure of hydrogen (kPa), k is the rate constant, K_1 is the adsorption equilibrium constant for methanol, and K_2 is the adsorption equilibrium constant for hydrogen. The constants in Eq. (6) are functions of temperature, as expressed in Eq. (7).

$$k = k_0 \exp\left(-\frac{E_R}{RT}\right),\ K_1 = K_{10}\exp\left(-\frac{\Delta H_1}{RT}\right),\ K_2 = K_{20}\exp\left(-\frac{\Delta H_2}{RT}\right) \tag{7}$$

E_R is the activation energy (J/mol), ΔH_1, and ΔH_2 are the heat of adsorption (J/mol) for methanol and hydrogen, and k_0 (mol m^{-2} s^{-1}), K_{10} (kPa^{-1}), and K_{20} (kPa^{-1}) are constants. These six parameters (k_0, E_R, K_{10}, ΔH_1, K_{20}, and ΔH_2) need to be determined for the plate catalyst by analyzing the data in Fig. 12. The method of analyzing the data is described in detail in [7].

The mass balance in the reactor is given by Eq. (8):

$$F_M^0 \frac{dX_M}{dA} = -r_M, \tag{8}$$

where F_M^0 is the molar flow rate of methanol (mol s^{-1}), X_M is the fractional methanol conversion, and A is the catalytic plate area (m^2), a variable running from 0 to A_T (total catalytic plate area in the reactor, equaling 4×10^{-3} m^2 for the studied reactor). For a given feed composition and reactor temperature, the exit conversion calculated by integrating Eq. (8) from 0 to A_T depends on the values of the six parameters in Eq. (7).

If correct values are provided for the integration of Eq. (8), the calculated and experimental conversions should be in good agreement. To determine the best fit of calculated conversions to experimental values, an objective function was defined (Eq. (9)) as

$$S=\Sigma_{i=1}^{N}(X_{c,i}-X_{e,i})^2, \quad (9)$$

where N is the number of experimental data points, $X_{e,i}$ is the i-th experimental conversion, and $X_{c,i}$ is the calculated conversion for conditions of the *i*-th experiment. The set of six parameters required to minimize the objective function was determined using the "fminsearch" function of MATLAB as follows (Eq. (10)):

$$k=7.57\times10^{9}\exp\left(-\frac{118\ \text{kJ mol}^{-1}}{RT}\right) \quad (\text{mol m}^{-2}\ \text{s}^{-1}),$$

$$K_1=5.34\times10^{-6}\exp\left(\frac{46.7\ \text{kJ mol}^{-1}}{RT}\right) \quad (\text{kPa}^{-1}) \quad (10)$$

$$K_2=1.07\times10^{-8}\exp\left(\frac{56.1\ \text{kJ mol}^{-1}}{RT}\right) \quad (\text{kPa}^{-1})$$

The lines in Fig. 12 represent conversions calculated using the above parameters.

6. Rate of COM over Cu-Zn(5)/AAO(24 h, PWT-HWT)

As OSRM is a combination of COM and SRM, the rate of COM can be obtained by analyzing OSRM data in Fig. 10 assuming the SRM reaction rate determined in the previous section. For such analysis, an OSRM reactor model is needed. As the reaction heat can be easily transferred through the metal (aluminum) part of the catalyst, the temperature along the length (2 cm) of each catalyst strip packed in the reactor can be assumed to be uniform, and an isothermal reactor model can be used in the present analysis.

As methanol is consumed by COM and SRM, the mass balance for methanol can be expressed as Eq. (11):

$$F_M^0\frac{dX_M}{dA}=-r_M-r_{COM}, \quad (11)$$

where r_{COM} is the methanol combustion rate. The oxygen in the reactor is consumed only by COM, and the corresponding mass balance can be expressed as Eq. (12):

$$F_O^0\frac{dX_O}{dA}=-1.5r_{COM}. \quad (12)$$

At O_2 conversions (X_O) below 0.6, only COM took place (Fig. 11), and the rate of steam reforming ($-r_M$) at this part of the catalyst equaled zero. As X_O increased over 0.6, SRM occurred together with COM until X_O=1, and the rate of SRM in OSRM could therefore be modeled as Eq. (13):

$$-r_M=0 \text{ when } X_O<0.6, \quad (13)$$
$$-r_M=\text{Eqs. (6) and (10) when } X_O\geq0.6.$$

For the combustion rate ($-r_{COM}$), a power law form was assumed (Eq. (14)):

$$-r_{COM}=A_0\exp\left(-\frac{E_C}{RT}\right)P_O^n \quad \text{mol m}^{-2}\ \text{s}^{-1}, \quad (14)$$

where P_O (partial pressure of oxygen, kPa), A_0 (pre-exponential factor), E_C (activation energy of combustion), and n (reaction order) are kinetic parameters that can be determined by fitting the calculated methanol conversion to experimental data in Fig. 10. Again, the "fminsearch" function of MATLAB was used to find parameters resulting in the best fit.

When the parameters from the best fit are substituted into Eq. (14), it becomes Eq. (15):

$$-r_{COM}=25800\exp\left(-\frac{75.2\ \text{kJ mol}^{-1}}{RT}\right)P_O^{0.0} \quad \text{mol m}^{-2}\ \text{s}^{-1} \quad (15)$$

Previously, combustion reaction orders of 0.14 [33] and 0.18 [40] were reported, which indicated a very weak dependence of the combustion rate on the partial pressure of oxygen. Herein, the COM rate was found to be independent of the oxygen partial pressure.

The lines in Fig. 10 show methanol conversions calculated using the developed OSRM reactor model (Eqs. (11) and (12)), and the good agreement between experimental and calculated conversions demonstrates the validity of the above OSRM reactor model and the equation expressing the COM rate (Eq. (15)).

CONCLUSIONS

We developed a Cu-based Al plate catalyst for OSRM, using an AAO layer grown on an Al plate by anodic oxidation in oxalic acid solution as the catalyst support to achieve strong binding of the catalyst layer; the specific surface area of this support was increased by pore widening and hot water treatments. The active metal loading and catalyst activity increased with increasing number of impregnations, with multiple impregnations (more than three times) required to achieve sufficiently high activity. Notably, catalytic activity slowly declined during the reaction, but could be fully restored by simple oxidation treatment. As the main body of the plate catalyst is highly thermally conductive Al, heat transfer through the catalyst structure is very rapid, and the catalyst structure as a whole can be assumed to be under isothermal conditions, which precludes the formation of a harmful hot spot in the reactor during OSRM.

OSRM was shown to be a combination of COM and SRM reactions, with COM being the only reaction at O_2 conversions below 0.6. Conversely, both SRM and COM reactions took place at O_2 conversions exceeding 0.6, and SRM was the only reaction occurring after full O_2 depletion. The rates of SRM and COM reactions were determined for the Cu-Zn(5)/AAO(24 h, PWT-HWT) catalyst.

ACKNOWLEDGEMENTS

This research was supported by the Basic Science Research Program of the National Research Foundation of Korea (NRF) funded by the Ministry of Education (2009-0093819). The authors thank Dr. Hideo Daimon at Toshisha University in Japan for assistance with SEM-EDX analysis.

REFERENCES

1. S. Golunski, *Energy Environ Sci.*, **3**, 1918 (2010).
2. B. J. Bowers, J. L. Zhao, M. Ruffo, R. Khan, D. Dattatraya and N. Dushman, *Int. J. Hydrogen Energy*, **32**, 1437 (2007).
3. J. K. Lee and D. Park, *Korean J. Chem. Eng.*, **15**, 658 (1998).
4. S. J. Kong, J. H. Jun and K. J. Yoon, *Korean J. Chem. Eng.*, **21**, 793 (2004).
5. J. H. Park, D. Lee, H. C. Lee and E. D. Park, *Korean J. Chem. Eng.*, **27**, 1132 (2010).
6. P. J. de Wild and M. J. F. M. Verhaak, *Catal. Today*, **60**, 3 (2000).

7. J. K. Lee, J. B. Ko and D. H. Kim, *Appl. Catal. A Gen.*, **278**, 25 (2004).
8. A. Iulianelli, P. Ribeirinha, A. Mendes and A. Basile, *Renew. Sust. Energy Rev.*, **29**, 355 (2014).
9. M. L. Cubeiro and J. L. G. Fierro, *J. Catal.*, **179**, 150 (1998).
10. Y. C. Lin, K. L. Hohn and S. M. Stagg-Williams, *Appl. Catal. A. Gen.*, **327**, 164 (2007).
11. J. Agrell, H. Birgersson, M. Boutonnet, I. Melián-Cabrera, R. M. Navarro and J. L. G. Fierro, *J. Catal.*, **219**, 389 (2003).
12. J. R. Lattner and M. P. Harold, *Catal. Today*, **120**, 78 (2007).
13. H. Y. Tang, J. Greenwood and P. Erickson, *Int. J. Hydrogen Energy*, **40**, 8034 (2015).
14. M. V. Twigg and M. S. Spencer, *Top. Catal.*, **22**, 191 (2003).
15. G. J. Cheng, A. B. Yu and P. Zulli, *Chem. Eng. Sci.*, **54**, 4199 (1999).
16. D. Wen and Y. Ding, *Chem. Eng. Sci.*, **61**, 3532 (2006).
17. D. H. Kim and J. Lee, *Stud. Surf. Sci.*, **159**, 685 (2006).
18. H. Masuda and K. Fukuda, *Science*, **268**, 1466 (1995).
19. A. P. Li, F. Muller, A. Birner, K. Nielsh and U. Gosele, *J. Vac. Sci. Technol. A*, **17**, 1428 (1999).
20. W. Lee and S.-J. Park, *Chem. Rev.*, **114**, 7487 (2014).
21. M. Mehmood, A. Rauf, M. A. Rasheed, S. Saeed, J. I. Akhter, J. Ahmad and M. Aslam, *Mater. Chem. Phys.*, **104**, 306 (2007).
22. G. Alcalá, P. Skeldon, G. Thompson, A. Mann, H. Habazaki and K. Shimizu, *Nanotechnology*, **13**, 451 (2002).
23. J. C. Ganley, K. L. Riechmann, E. G. Seebauer and R. I. Masel, *J. Catal.*, **227**, 26 (2004).
24. L. Zhou, Y. Guo, M. Yagi, M. Sakurai and H. Kameyama, *Int. J. Hydrogen Energy*, **34**, 844 (2009).
25. L. Wang, T. P. Tran, D. V. Vo, M. Sakurai and H. Kameyama, *Appl. Catal. A.*, **350**, 150 (2009).
26. E. Linga Reddy, J. Karuppiah, H. C. Lee and D. H. Kim, *J. Power Sources*, **268**, 88 (2014).
27. E. Linga Reddy, H. C. Lee and D. H. Kim, *Int. J. Hydrogen Energy*, **40**, 2509 (2015).
28. T. P. Tran, Y. Guo, J. Chen, L. Zhou, M. Sakurai and H. Kameyama, *J. Chem. Eng. Japan*, **41**, 1042 (2008).
29. J. Zhang, J. Kielbasa and D. L. Carroll, *Mater. Chem. Phys.*, **122**, 295 (2010).
30. Y. Guo, L. Zhou and H. Kameyama, *Chem. Eng. J.*, **168**, 341 (2011).
31. J. W. Evans, M. S. Wainwright, A. J. Bridgewater and D. J. Young, *Appl. Catal.*, **7**, 75 (1983).
32. C. Fukuhara, H. Ohkura, Y. Kamata, Y. Murakami and A. Igarashi, *Appl. Catal. A Gen.*, **273**, 125 (2004).
33. J. H. Kim, Y. S. Jang and D. H. Kim, *Chem. Eng. J.*, **338**, 752 (2018).
34. A. J. Marchi, J. L. G. Fierro, J. Santamaría and A. Monzón, *Appl. Catal. A Gen.*, **142**, 375 (1996).
35. T. J. Huang and S. L. Chren, *Appl. Catal.*, **40**, 43 (1988).
36. S. Velu, K. Suzuki, M. Kapoor, F. Ohashi and T. Osaki, *Appl. Catal. A Gen.*, **213**, 47 (2001).
37. L. A. Espinosa, R. M. Lago, M. A. Pena and J. L. G. Fierro, *Top. Catal.*, **22**, 245 (2003).
38. M. Turco, G. Bagnasco, C. Cammarano, P. Senese, U. Costantino and M. Sisani, *Appl. Catal. B Environ.*, **77**, 46 (2007).
39. J. Kim, J. Byeon, I. G. Seo, H. C. Lee, D. H. Kim and J. Lee, *Korean J. Chem. Eng.*, **30**, 790 (2013).
40. T. L. Reitz, S. Ahmed, M. Krumpelt, R. Kumar and H. H. Kung, *J. Mol. Catal. A Chem.*, **162**, 275 (2000).
41. J. Agrell, M. Boutonnet and J. L. G. Fierro, *Appl. Catal. A Gen.*, **253**, 213 (2003).